Analysis of the DC performance of the ITER CSI coil using the 4C code

Analysis of the DC performance of the ITER CSI coil using the 4C code

Roberto Bonifetto[a], Takaaki Isono[b], Nicolai Martovetsky[c], Laura Savoldi[a], Roberto Zanino[a]

[a]*NEMO Group, Dipartimento Energia, Politecnico di Torino, Torino, Italy*
[b]*National Institutes for Quantum and Radiological Science and Technology (QST), Naka, Japan*
[c]*US ITER Project Office, Oak Ridge (TN), United States*

The DC performance of the ITER Central Solenoid Insert (CSI) coil, a single layer solenoid wound using the same Nb_3Sn conductor that will be adopted for the 3L module of ITER CS, was measured during the 2015 test campaign in different magnetic field and current operating conditions, before and after electromagnetic and thermal cycles, as well as before and after quench tests. The 4C thermal-hydraulic code is applied here to the analysis of the CSI performance: first, the free parameters of the model are calibrated; then, the model is validated against measurements not used for its calibration. The model is then used to compute the current sharing temperature, to be compared with the measured jacket temperature, and to assess the performance after quench tests.

Keywords: ITER, superconducting magnets, Nb_3Sn, current sharing temperature, thermal-hydraulic analysis.

1. Introduction

In 2015, the ITER Central Solenoid Insert (CSI) coil [1], whose Nb_3Sn cable-in-conduit conductor (CICC) will be adopted for the 3L module of the ITER CS, has been successfully tested [2] in the bore of the ITER Central Solenoid Model Coil (CSMC) [3], at the National Institutes for Quantum and Radiological Science and Technology (former JAEA) center of Naka, Japan. The test of the CSI DC performance allowed assessing its current sharing temperature (T_{CS}) after up to 16 thousand electromagnetic (EM) cycles and 3 thermal cycles (warm-up / cool-down), as well as after the quench tests carried out at the end of the campaign [4]. The T_{CS} was measured in different operating conditions in terms of magnetic field and current, corresponding to different phases of the ITER plasma pulse, namely initial magnetization (IM) and end of burn (EoB), see table 1. As a full-size short sample of the same CICC was previously tested in the SULTAN facility, SULTAN-like operating conditions were also reproduced to allow a comparison, with special reference to the effect of the Hoop strain, not present in the SULTAN straight sample tests.

The 4C code [5], recently applied to the analysis of slow (cool-down [6]) and fast (dump [7], stability [8] and quench [4]) transients in the CSI, is used here to analyze the CSI DC performance. The free parameters of the 4C model (the effective n-value of the conductor and the "extra" longitudinal strain ε_{extra} [9]) are first calibrated using the voltage and jacket temperature (T_{jk}) measured by a subset of the available sensors. The values of n and ε_{extra} are then frozen and the model is validated against data measured by other sensors. The T_{CS} values computed by 4C before and after EM cycling and quenches are reported and, when applicable, compared to the SULTAN results, as well as to the results of previous work by other authors.

2. Experimental setup

The CSI is a nine-turn, single layer solenoid wound with a ~43 m long CICC [1]. It is well instrumented from the thermal-hydraulic and electrical point of view [4], see figure 1a. The central turn, located in the highest field region, is equipped with five voltage taps and thermometers and two "star" voltage (VS) sensors, see figure 1b. The latter are six pairs of taps located in different azimuthal positions on the jacket external sides, see figure 1c, at two cross sections. The spacing between the "star" voltage sensors is 0.45 m.

Table 1. Testing conditions for the CSI performance (B_{peak} = peak magnetic field including background field and self-field, BoC = beginning of EM cycling, EoC = end of EM cycling, AQ = after quenches, the subscript "1" and "2" refer to T_{CS} measurements before and after the 7 s delay quench [4], respectively).

	EoB	IM	SULTAN-like
I_{CSMC} [kA]	42.8	44.8	39.2
B_{peak} [T]	12.6	13	11.5
I_{CSI} [kA]	45.1	40	45.1
$I_{CSI}\times B_{peak}$ [kA×T]	568	520	519
BoC (shot #)	61-2	58-2	55-2
EoC (shot #)	176-2	160-2	161-2
AQ_1 (shot #)	-	187-2	-
AQ_2 (shot #)	-	194-2	-

The desired test conditions are reached ramping-up the transport current in the CSMC (I_{CSMC}), to produce the background magnetic field (see table 1), and then that in the CSI (I_{CSI}). Starting from an operating thermal-hydraulic condition of inlet temperature T_{in} ~4.5 K, pressure p_{in} ~6 bar and mass flow rate dm/dt_{in} ~10 g/s, T_{in} is increased step by step with a resistive heater located on the pipe upstream of the coil inlet, see figures 1a, 2a; consequently, dm/dt_{in} is gradually reduced due to the density change, see again figure 2a. The time between the T_{in} steps is long enough (~10-15 min) to let the temperature in the central turns stabilize. When T increases above T_{CS}, the voltage takes off as reported in figure 2b (the cable T_{CS} is conventionally reached when the electric field locally reaches 10 μV/m for the first time, i.e. 4.5 μV are measured by the VS sensors in figure 2b). T_{in} is increased until ~50 μV/m are measured

author's email: roberto.bonifetto@polito.it

on the central VD1011 sensor; then the I_{CSI} is rapidly (–4 kA/min) reduced to 0 kA, to avoid the quench of the coil, see figure 2b.

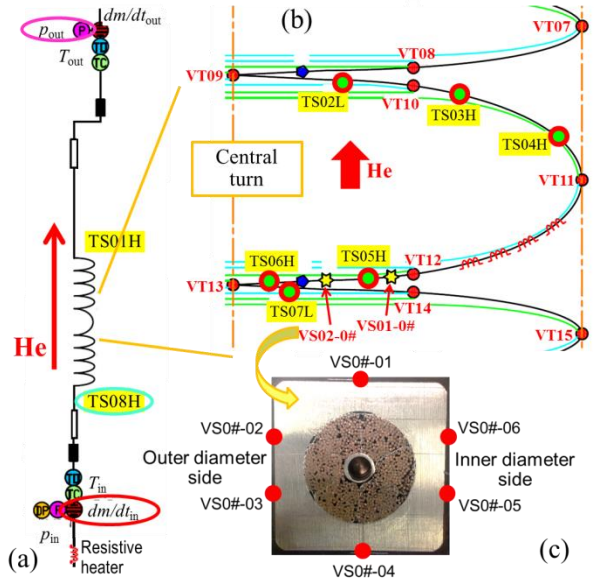

Fig. 1. CSI instrumentation relevant for the DC performance tests. (a) Inlet and outlet thermometers, pressure taps and flow meters. (b) Zoom on the central turn instrumentation, including several thermometers (TS) and voltage taps (VT). (c) Location of VS sensors.

3. 4C model

The general 4C model of the CSI is described in detail in [6]. However, as we focus here on the central turn, since that is where the minimum margin is located, the role played by the spacers and by the other steel structures is negligible and the external side of the jacket can be considered adiabatic.

The magnetic field amplitude [10], see figure 3, is assumed to vary linearly from the average value on the cable axis to the peak value at the conductor inner radius. The total axial strain ε_{tot} is computed as

$$\varepsilon_{tot} = \varepsilon_{th} + \varepsilon_{hoop} + \varepsilon_{extra} \qquad (1)$$

where ε_{th} is the thermal strain (estimated by extrapolation to be –0.59% [11]) due to different thermal contraction of jacket and strands after heat treatment, ε_{hoop} is the hoop strain, directly proportional to $I_{CSI}\times B$ as reported in [11] and ε_{extra} is here a fitting parameter of the model [9] possibly related to the axial strain induced by lateral forces crushing the strands against each other and consequently bending them [11], rather than to an irreversible degradation of the strands. Both the magnetic field and ε_{tot} are used in the calculation of the cable critical current I_C by means of the ITER scaling [12] with the parameters reported in [11]. The critical current enters equation 2 for the calculation of the electric field E:

$$E = E_0 \left(\frac{I_{CSI}}{I_C}\right)^n \qquad (2)$$

where E_0 is the critical field (10 μV/m) and n is the conductor n-value, the second fitting parameter of the model.

In view of the long transient and of the negligible role played by the circuit, measured boundary conditions (marked with ellipses in figure 1a) are adopted at the CSI inlet (T_{in} and dm/dt_{in}) and outlet (p_{out}). The simulation follows the whole T_{CS} measurement reported in figure 2.

In the simulations, first the free parameters of the code (n and ε_{extra}) are calibrated by comparison with experimental data, following the same optimization strategy adopted in [9]: the parameters' space $5 < n < 10$ and $-0.04\% < \varepsilon_{extra} < 0\%$ is scanned with a set of simulations; the $V(T)$ experimental and computed curves are compared in the range 5 μV/m - 40 μV/m. The best fitting parameters n^{opt} and ϵ_{extra}^{opt} are obtained minimizing the relative difference σ between the simulation and measurement. n^{opt} and ϵ_{extra}^{opt} are then frozen and used to assess the T_{CS} by means of the 4C code, computing the strand temperature at the location where the 10 μV/m are reached first.

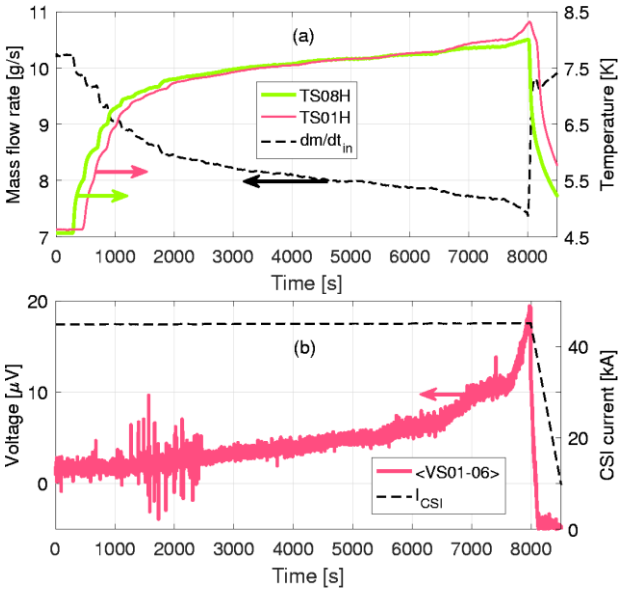

Fig. 2. Evolution of experimental data from T_{CS} measurement at EoC in SULTAN-like conditions. (a) Inlet (TS08H) and outlet (TS01H) jacket temperature (solid, right axis) and inlet mass flow rate (dashed, left axis). (b) Average of VS sensors (solid, left axis) and current in the CSI (dashed, right axis).

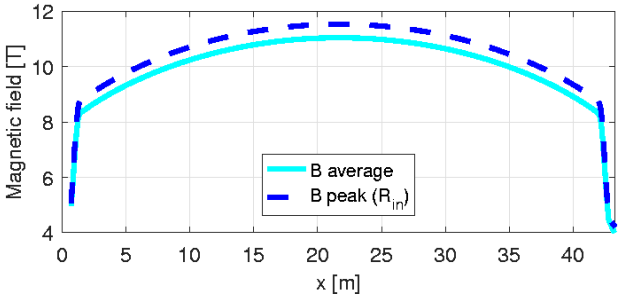

Fig. 3. Distribution of the magnetic field amplitude (left axis), on the cable axis and at the conductor inner radius, in SULTAN-like conditions [10].

4. Results

In order to better identify the cable T_{CS}, the results are reported in the *V-T* plane: the voltage is filtered to remove oscillations and zeroed at $T < 5.5$ K. Figure 4 shows the average of the 6 VS taps (see figure 1c) vs. TS05H, in SULTAN-like conditions, at both BoC and EoC.

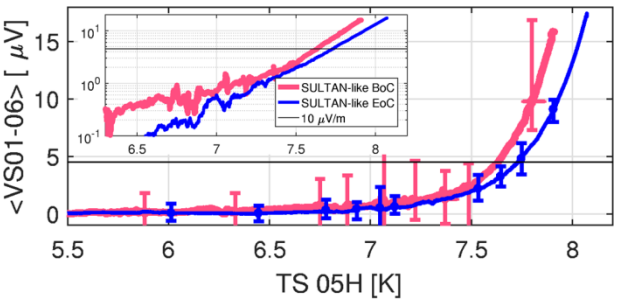

Fig. 4. Measured *V-T* curve for SULTAN-like T_{CS} tests at both BoC (thick pink line) and EoC (thin blue line). The error bar is due to the high frequency oscillations in both *V* and *T* signals, during the temperature plateau, see figure 2b. The same plot is reported with voltage in logarithmic scale in the inset. The 10 μV/m threshold is also reported (horizontal thin black line).

The comparison between the two *V-T* curves in figure 4 highlights the (slight) T_{CS} increase measured after EM cycles, while in the inset the representation of the voltage in logarithmic scale shows the (small) *V-T* slope reduction.

For each test condition analyzed here, see table 1, the model is calibrated using the (average) voltage measured by the VS sensors. The resulting n^{opt} and ϵ_{extra}^{opt} values, obtained from the best fit of the experiment, are reported in table 2. In all conditions, n^{opt} is reduced after EM cycles, and, as already observed in [9], it is much lower that the strand *n*-value [13], as expected [14, 15]. While the differences between n^{opt} and ϵ_{extra}^{opt} at BoC are not fully relevant in view of the possible current and strain non-uniformities in the virgin conductor, at EoC the effect of *I*×*B* on ϵ_{extra}^{opt} is evident: as already observed in [9], to higher *I*×*B* corresponds a higher (in absolute value) ϵ_{extra}^{opt}, see also table 1. The ε_{hoop} computed according to the fit in [11] is ~0.07% at EoB and ~0.065% at IM and SULTAN-like conditions, respectively. Table 2 also confirms that ε_{hoop} and ε_{extra} almost compensate each other, well in agreement with the fit reported in [11] and thus confirming the physical interpretation of that component of the total strain reported there. Note that the absolute value of ϵ_{extra}^{opt} is not monotonically increasing with EM cycles, confirming that no irreversible degradation of the strands is observed. The comparison between the computed T_{CS} (strand temperature) and the corresponding T_{jk} (to be compared with the measured values) shows a difference of ~10 mK, confirming that the CSI instrumentation is fully adequate for the DC performance assessment.

The effect of quenches is negligible on the ϵ_{extra}^{opt}, while a variation of ~1 in the n^{opt} is registered. The conductor *n*-value can then be estimated to be ~6-7, depending on the conditions. This confirms the value $n = 7$ currently used for ITER CS analyses.

Table 2. Values of n^{opt} and ϵ_{extra}^{opt} [%] obtained from the best fit of experimental data.

	EoB		IM		SULTAN-like	
	n^{opt}	ϵ_{extra}^{opt}	n^{opt}	ϵ_{extra}^{opt}	n^{opt}	ϵ_{extra}^{opt}
BoC	7.5	–0.07	9.3	–0.07	7.5	–0.08
EoC	6.8	–0.09	5.8	–0.07	7.0	–0.06
AQ_1	-	-	6.8	–0.07	-	-
AQ_2	-	-	6.0	–0.07	-	-

After the calibration of the free parameters, the model and the best fit procedure are validated by comparison of the simulation results with all the *V-T* characteristics measured along the central turn. The agreement, not guaranteed *a priori* in view of the local magnetic field (see table 3) and strain variation, as well as in the different relative distance among temperature sensors and voltage taps, is excellent in all cases, as documented by the comparison between figures 5a and 5b. In particular for sensors "B" and "C" the simulation is able to capture the experimental T_{CS} well within the 10 mK difference quoted in table 3.

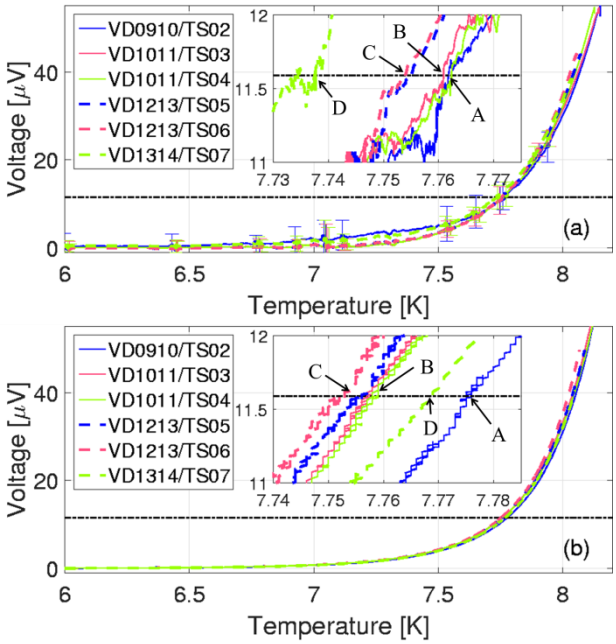

Fig. 5. Experimental (a) and computed (b) *V-T* curves for SULTAN-like T_{CS} tests at EoC for all the available *V* and *T* sensors in the central turn. The insets are zooms around the T_{CS} region (letters correspond to the rows of table 3). The 10 μV/m threshold is also reported (horizontal dash-dotted thin blue line).

Figure 5a shows that all *V-T* characteristics measured on the central turn look quite similar. This confirms that the SC properties of the CSI conductor are uniform as expected/desired, at least over the whole central turn, and the CSI cable behavior is similar to that of a single strand with proper average properties. Table 3 reports the T_{CS} computed from the average magnetic field and strain between the *V* sensors of the central turn: the different values are justified by small *B* variations, while the non-monotonic T_{CS} distribution along the CSI (with a minimum between the VT12 and VT13 taps) is due to the presence of a peak in the magnetic field (close to VT12). The same non-monotonicity is observed also in the computed *V-T*

characteristics, see the inset of figure 5b. In the experiment, see the inset of figure 5a, only VD1314 sensor (D) shows a slightly lower T_{CS} than expected, while all other sensors are in perfect agreement with the computed ones and the estimations in table 3.

Also the computed TS03H evolution (at the outlet of the central turn) was compared with the experimental one, showing an excellent agreement (not shown) and confirming the suitability of the code to follow the whole T_{CS} measurement transient.

Table 3. T_{CS} (B_{ave}, ε_{ave}, j) estimation for the different V sensors in the central turn (current density j = 285 A/mm^2).

	VD	B_{ave} [T]	ε_{ave} [%]	T_{CS} [K]
A	09-10	11.001	–0.59	7.78
B	10-11	11.027	–0.59	7.76
C	12-13	11.033	–0.59	7.75
D	13-14	11.015	–0.59	7.77

Table 4. Values of T_{CS} [K] computed by the 4C code compared with previous analyses by other authors.

	EoB		IM		SULTAN-like	
	4C	[11] // [16]	4C	[11] // [16]	4C	[11] // [16]
BoC	6.89	6.8 // 6.89	6.72	6.68 // 6.72	7.61	7.6 // 7.64
EoC	6.8	6.97 // 6.82	6.75	6.76 // 6.76	7.75	7.72 // 7.72
AQ_1	-	-	6.74	-	-	-
AQ_2	-	-	6.74	-	-	-

Table 4 reports the T_{CS} computed by the 4C code, always within (or very close to) the range of results obtained by other analyses [11, 16]. This is not straightforward, as the computed T_{CS} is the results of complex thermal-hydraulic calculations where an important role is played by semi-empirical heat transfer correlations and critical current scaling laws. The minimum T_{CS} is measured in IM conditions, where the magnetic field is maximum, even if the transport current is lower than in EoB conditions. In SULTAN-like conditions, the measured T_{CS} on the CSI is ~0.5-0.6 K higher with respect to SULTAN sample measurements (~6.9-7 K at BoC, ~7.2-7.3 K at EoC [13]): as expected, the coiled CSI benefits indeed of the (positive) ε_{hoop} that reduces in absolute terms the (negative) ε_{th} [11]. The EM cycles induced a small T_{CS} increase in SULTAN-like conditions (~150 mK), while the increase is much smaller at IM (~50 mK). At EoB the T_{CS} is slightly reduced (~100 mK) after cycling. Globally, there is no remarkable effect of EM and thermal cycling on T_{CS}, confirming the excellent performance of the short twist pitch cable pattern adopted for this conductor [17, 18].

The performance after quench tests (AQ_1) has also been assessed, for the first time, showing no changes with respect to the EoC conditions, even after the tests with 7 s delay (AQ_2) [4], see again table 4. This, together with the satisfaction of the hot spot criteria reported in [4], may open the possibility to extend the quench detection time in the ITER CS quench detection system without reducing the conductor performance.

5. Conclusions and perspective

The 4C code has been applied to the analysis of the DC performance of the ITER CSI coil tested in 2015 at QST.

After calibrating the free parameters of the model on a small subset of the experimental data, the model was validated against the other available diagnostics, proving to be able to follow the whole T_{CS} measurement transient. The detailed simulations also confirmed for the first time that the measured jacket temperature can be reliably used to assess the cable T_{CS}.

The estimated conductor n-value (~6-7 after EM cycles) is in agreement with that used so far in ITER CS analyses.

The T_{CS} analysis allowed to assess the performance after quench tests: no relevant T_{CS} variation is observed.

The SC properties of the CSI conductor were also confirmed to be uniform as expected/desired, at least over the whole central turn.

The validation of both the model and the procedure adopted to assess the T_{CS} will allow to reliably apply the code to the analysis of the DC performance of the less instrumented ITER CS module that is going to be tested in the next years.

Acknowledgments

The work of RB was financially supported by a EUROfusion post-doctoral fellowship. The authors thank QST Naka for kind hospitality during the CSI tests.

References

[1] T. Isono et al., Fabrication of an Insert to Measure Performance of ITER CS Conductor, IEEE Trans. Appl. Supercond. 25 (3) (2015) 4201004.

[2] N. Martovetsky et al., ITER Central Solenoid Insert Test Results, IEEE Trans. Appl. Supercond. 26 (4) (2016) 4200605.

[3] H. Tsuji et al., Progress of the ITER Central Solenoid Model Coil program, Nuclear Fusion 41 (2001) 645-651.

[4] R. Bonifetto et al., Analysis of Quench Propagation in the ITER Central Solenoid Insert (CSI) Coil, presented at ASC and submitted to IEEE Trans. Appl. Supercond. (2016).

[5] L. Savoldi Richard, F. Casella, B. Fiori and R. Zanino, The 4C code for the cryogenic circuit conductor and coil modeling in ITER, Cryogenics 50 (3) (2010) 167-176.

[6] R. Bonifetto et al., Analysis of the cooldown of the ITER Central Solenoid Model Coil and Insert Coil, submitted to SUST (2016).

[7] M. Breschi et al., Analysis of AC losses in the ITER Central Solenoid Insert (CSI) Coil, presented at ASC and submitted to IEEE Trans. Appl. Supercond (2016).

[8] L. Savoldi et al., Analysis of the ITER Central Solenoid Insert (CSI) Coil Stability Tests, presented ad TOFE and submitted to SUST (2016).

[9] R. Zanino, N. Mitchell and L. Savoldi Richard, Analysis

and interpretation of the full set (2000–2002) of T_{CS} tests in conductor 1A of the ITER Central Solenoid Model Coil, Cryogenics 43 (2003) 179-197.
[10] A. Khodak, private communication, 17 October 2015.
[11] N. Martovetsky et al., Characterization of the ITER CS conductor and projection to the ITER CS performance, presented at SOFT and submitted to Fus. Eng. Des. (2016).
[12] L. Bottura and B. Bordini, Jc (B, T, ε) Parameterization for the ITER Nb3Sn Production, IEEE Trans. Appl. Supercond. 19 (3) (2009) 1521-1524
[13] Naka Fusion Institute Superconducting Test Group, Database of CS Insert Coil Experiment in 2015, National Institutes for Quantum and Radiological Science and Technology report (2015), unpublished results.
[14] N. Martovetsky, Correlation between degradation and broadness of the transition in CICC, Supercond. Sci. Technol. 26 (2013) 104001.
[15] A. Shikov et al., Development of the Nb_3Sn Bronze Strand of TF Conductor Sample for Testing in SULTAN Facility, IEEE Trans. Appl. Supercond. 19 (3) (2009) 1466-1469.
[16] M. Bianchi and M. Breschi, Tcs, Ic and effective strain of the CSI, presented at CSI Test Results Meeting, Naka, 26-28 Oct. 2015.
[17] D. Bessette, Design of a Nb_3Sn Cable-in-Conduit Conductor to Withstand the 60 000 Electromagnetic Cycles of the ITER Central Solenoid, IEEE Trans. Appl. Supercond. 24 (3) (2014) 4200505.
[18] Y. Nabara et al., Impact of Cable Twist Pitch on T_{cs}-Degradation and AC Loss in Nb_3Sn Conductors for ITER Central Solenoids, IEEE Trans. Appl. Supercond. 24 (3) (2014) 4200705.